2000

# Two-Dimensional Ferroelectrics

L. M. Blinov
*Institute of Crystallography, Russian Academy of Sciences, Leninski¦¯ prosp. 59, 117333 Moscow, Russian Federation*

V. M. Fridkin
*Institute of Crystallography, Russian Academy of Sciences, Leninski¦¯ prosp. 59, 117333 Moscow, Russian Federation*

S.P. Palto
*Institute of Crystallography, Russian Academy of Sciences, Leninski¦¯ prosp. 59, 117333 Moscow, Russian Federation*

A. V. Bune
*University of Nebraska - Lincoln*

Peter A. Dowben
*University of Nebraska-Lincoln*, pdowben@unl.edu

*See next page for additional authors*

*Physics – Uspekhi* **43** (3) 243 – 257 (2000) 

*REVIEWS OF TOPICAL PROBLEMS* PACS numbers: **75.70. – i**, **77.80. – e**

# Two-dimensional ferroelectrics

L M Blinov, V M Fridkin, S P Palto, A V Bune, P A Dowben, S Ducharme

DOI: 10.1070/PU2000v043n03ABEH000639

## Contents



**Abstract. The investigation of the finite-size effect in ferroelectric crystals and films has been limited by the experimental conditions. The smallest demonstrated ferroelectric crystals had a diameter of $\sim$ 200 A and the thinnest ferroelectric films were $\sim$ 200 A thick, macroscopic sizes on an atomic scale. Langmuir – Blodgett deposition of films one monolayer at a time has produced high quality ferroelectric films as thin as 10 A, made from polyvinylidene fluoride and its copolymers. These ultrathin films permitted the ultimate investigation of finite-size effects on the atomic thickness scale. Langmuir – Blodgett films also revealed the fundamental two-dimensional character of ferroelectricity in these materials by demonstrating that there is no so-called critical thickness; films as thin as two monolayers (1 nm) are ferroelectric, with a transition temperature near that of the bulk material. The films exhibit all the main properties of ferroelectricity with a first-order ferroelectric – paraelectric phase transition: polarization hysteresis (switching); the jump in spontaneous polarization at the phase transition temperature; thermal hysteresis in the polarization; the increase in the transition temperature with applied field; double hysteresis above the phase transition temperature; and the existence of the ferroelectric critical point. The films also exhibit a new phase transition associated with the two-dimensional layers.**

**L M Blinov, V M Fridkin, S P Palto** Institute of Crystallography, Russian Academy of Sciences,
Leninskiĭ prosp. 59, 117333 Moscow, Russian Federation
Tel. (7-095) 135 15 00. Fax (7-095) 135 10 11
E-mail: fridkin@ns.crys.ras.ru
**A V Bune, P A Dowben, S Ducharme** Department of Physics and Astronomy, Behlen Laboratory of Physics, Center for Materials Research and Analysis, University of Nebraska – Lincoln,
Lincoln, NE 68588-0111, USA
Tel. 402-472-8590. Fax 402-472-2879
E-mail: sducharme1@unl.edu

Received 8 August 1999
*Uspekhi Fizicheskikh Nauk* **170** (3) 247 – 262 (2000)
Translated by V M Fridkin; edited by S N Gorin

## 1. Introduction

Ultrathin crystalline films offer the possibility of exploring phase transitions in the crossover region between two and three dimensions. Second-order ferromagnetic phase transitions have been observed in monolayer magnetic films [1, 2], where the surface anisotropy energy stabilizes the two-dimensional ferromagnetic state at finite temperatures [3]. Similarly, a number of magnetic materials have magnetic surface layers that show a second-order ferromagnetic – paramagnetic phase transition with an increased Curie temperature [4]. Ferroelectricity is in many ways analogous to ferromagnetism, and bulk ferroelectricity and finite-size effects have been observed in nanocrystals as small as $\sim$ 200 A in diameter [5, 6], and in thin films as thin as 600 A [7] †. First-order ferroelectric – paraelectric phase transitions in surface layers approximately 200 A thick have been reported by Scott et al. [8] and found to have enhanced transition temperatures. These results also can be interpreted as bulk ferroelectricity suppressed by the effects of surface energy and the depolarization field, and imply that the bulk ferroelectric state is associated with a minimum critical size [8 – 10]. Nevertheless, it is clear that the ferroelectric phase transition in the two-dimensional lattice is possible even in the simplest two-dimensional Ising model, as shown by Onsager in 1944 [11].

Here, we present a review of investigations of the ferroelectric phase transition in crystalline films of a random copolymer of vinylidene fluoride and trifluoroethylene as thin as 10 A (two monolayers) prepared by Langmuir – Blodgett (LB) deposition. The first-order ferroelectric phase transition with a Curie temperature nearly equal to the bulk value was observed even in these essentially two-dimensional films. In addition, we observed a second phase transition at a lower temperature, which seems to have a surface nature. The absence of finite-size effects on the bulk transition implies

† And possibly as thin as 100 A, see Karasawa J et al. *Integrated Ferroelectrics* **12** 105 (1996). (*Authors' note for English Edition.*)

that these films must be considered as two-dimensional ferroelectrics.

## 2. Ferroelectricity and the ferroelectric phase transitions

Ferroelectric materials have fascinated scientists since their discovery in 1920 [12 – 15]. In analogy with ferromagnets, the characteristic properties of ferroelectrics include spontaneous electric polarization, polarization reversal (switching), and disappearance of the polarization above a ferroelectric phase transition temperature $T_c$. Ferroelectric materials have been a fertile field for the study of phase transitions, electron – phonon interactions, polaritons, and other optical and electrical phenomena in condensed matter.

From the time of the first reports of Valasek in the early 1920s [12, 16], many books and reviews have been devoted to the problem of ferroelectricity [14, 15, 17 – 19]. V L Ginzburg developed the first phenomenological theory of ferroelectricity in the 1940s [20, 21] based on the Landau theory of second-order phase transitions [22 – 24] and a similar treatment was developed by Devonshire shortly thereafter [13, 25, 26]. Later, many phenomenological aspects of the problem were developed by E M Lifshitz, V L Ginzburg, A P Levanyuk, D G Sannikov, V L Indenbom, and others. Here, we are giving only a short summary of the Landau – Ginzburg phenomenological treatment of the ferroelectric phase transitions.

Presuming that the order parameter in the Landau theory has the same transformation properties as the polarization vector $P$, we can in the uniaxial case express the Gibbs free energy density $G$ in the Landau – Ginzburg polynomial expansion

$$G = F - EP = F_0 + \frac{\alpha}{2} P^2 + \frac{\beta}{4} P^4 + \frac{\gamma}{6} P^6 - EP, \qquad (2.1)$$

where $F_0$ is the free energy density of the paraelectric phase (when $E = 0$), $E$ is the electric field, and the expansion coefficients $\alpha$, $\beta$ and $\gamma$ are in general temperature and pressure dependent. The equilibrium conditions correspond to the minimum of the free energy density, where

$$\frac{\partial F}{\partial P} = 0, \qquad \frac{\partial^2 F}{\partial P^2} > 0. \qquad (2.2)$$

The two main categories of ferroelectric materials are those that undergo a second-order transition, like triglycine sulfate (TGS), and those that undergo a first-order transition, like $BaTiO_3$ and other perovskites.

In the Landau – Ginzburg theory of second-order ferroelectric phase transitions, the expansion coefficients have the values

$$\alpha = \frac{1}{\varepsilon_0 C}(T - T_0), \qquad \beta > 0, \qquad \gamma = 0, \qquad (2.3)$$

where $T_0 > 0$ is the Curie temperature, $C > 0$ is the Curie – Weiss constant, and $\varepsilon_0$ is the permittivity of free space. Applying the equilibrium conditions (2.2) and the coefficients (2.3) to the free energy density expansion (2.1), we obtain the value of the spontaneous polarization in the ferroelectric phase

$$P_s = P(E = 0) = \pm\sqrt{\frac{\alpha}{\beta}} = \pm\sqrt{\frac{1}{\beta C \varepsilon_0}(T - T_0)}, \qquad T < T_0. \qquad (2.4)$$

The equilibrium temperature of transition from paraelectric to ferroelectric phase is $T_c = T_0$; all properties are dependent on the difference between the crystal temperature $T$ and the phase transition temperature $T_c$. The $\pm$ signs indicate that the polarization can point in either direction along the symmetry axis (recall that this is the uniaxial case), and correspond to the two energetically equivalent states of the ferroelectric crystal at zero electric field. Equation (2.4) shows the typical result that at the second-order ferroelectric phase transition there is no jump in the order parameter (the magnitude $P_s$ in this case) and in the latent heat of transition. However, there is a jump in the heat capacity.

The dielectric polarizability $\chi$ in the paraelectric phase is built-in to the definition of $\alpha$ and calculated from the free energy density expansion (2.1) and equilibrium conditions (2.2):

$$\frac{\partial^2 F}{\partial P^2} = \frac{1}{\chi} = \frac{T - T_0}{\varepsilon_0 C}.$$

The dielectric constant of the medium $\varepsilon = \varepsilon_\infty + \chi/\varepsilon_0$ contains contributions from the background polarizability and the ferroelectric polarizability (2.5).

The general first-order phase transition is accompanied by a small but finite jump of the order parameter $P$ and enthalpy. Many ferroelectric materials exhibit a special kind of first-order phase transition with a change of symmetry from a group to subgroup, which is close to the situation in the second-order transition, and can be described by the free-energy density (2.1) with a negative $P^4$ term (negative $\beta$) and a nonzero $P^6$ (positive $\gamma$) term,

$$\alpha = \frac{1}{\varepsilon_0 C}(T - T_0), \qquad \beta < 0, \qquad \gamma > 0. \qquad (2.5)$$

The phase transition temperature is

$$T_c = T_0 + \frac{3\varepsilon_0}{16}\beta^2 \frac{C}{\gamma},$$

and below this temperature the equilibrium spontaneous polarization is

$$P_s = P(E = 0) = \pm\sqrt{-\frac{\beta}{2\gamma}\left(1 + \sqrt{1 - t}\right)}, \qquad T < T_0, \qquad (2.6)$$

where the reduced temperature is

$$t = \frac{4\alpha\gamma}{\beta^2} = \frac{4\gamma(T - T_0)}{\varepsilon_0 C \beta^2}.$$

There is a jump in the magnitude of the spontaneous polarization from zero by $\Delta P_s = \sqrt{-3\beta/4\gamma}$ at the phase transition temperature $T_c$ (for $E = 0$).

Another typical feature of the first-order phase transition is the temperature hysteresis and the metastable coexistence of both phases in the vicinity of the transition temperature $T_c$. The maximum temperature hysteresis in zero field $\Delta T = \varepsilon_0 C \beta^2/4\gamma$ is a range bounded by $T_0$, the lower temperature limit for the metastable existence of the nonpolar state, and $T_0 + \Delta T$, the upper limit for the metastable existence of the polar state. The transition temperature $T_c$ falls in between these two limits.

The electric field is calculated directly from the free energy density (2.1),

$$E = \frac{\partial G}{\partial P} = \alpha P + \beta P^3 + \gamma P^5 . \tag{2.7}$$

This nonlinear dependence of the polarization $P$ on the electric field $E$ leads to a hysteresis loop, which is one of the key characteristics of ferroelectric materials. The hysteresis loop shown in Fig. 1 for the ferroelectric state ($T < T_c$) illustrates the bistable nature of the polarization over a range of electric fields. The positive and negative values of the polarization correspond to the equivalent minima in the free energy. The intrinsic ferroelectric coercive field is the magnitude of the positive or negative electric field at which the polarization becomes single-valued and reverses direction, as shown by the arrows in Fig. 1. The measured extrinsic coercive fields in real ferroelectric materials are orders of magnitude smaller than the intrinsic value calculated from the Landau–Ginzburg theory, because the theory does not take into account the extrinsic mechanism of local polarization reversal by nucleation followed by domain propagation and growth.

The contribution of the polarization to the dielectric polarizability $\chi$ in the paraelectric and ferroelectric phases is calculated from the electric field expression (2.7) as follows:

$$\frac{\varepsilon_0}{\chi} = \left[\frac{\partial^2 F}{\partial P^2}\right] = \frac{T - T_0}{C} , \qquad T > T_0 ,$$
$$\frac{\varepsilon_0}{\chi} = \left[\frac{\partial^2 F}{\partial P^2}\right] = \frac{8(T - T_0)}{C} + \frac{9}{4}\frac{\beta^2}{\gamma} , \qquad T < T_0 . \tag{2.8}$$

It was mentioned above that the expansion coefficients of the free energy expansion (2.1) depend on temperature $T$ and pressure $p$. Landau showed that, along the curve in the $p, T$ diagram separating phases of different symmetry, there is a critical point $p_{cr}$, $T_{cr}$ that marks the boundary between first- and second-order phase transitions, that is, the coefficient $\beta$ of the $P^4$ term changes sign. The Landau–Ginzburg theory very well describes the anomalies near this co-called 'critical Curie point' or 'tricritical point' [19]. The first experimental observations of the tricritical point were reported in 1968 [27, 28]. In the first paper [27], it was shown that in SbSI crystals, which show a phase transition of the first order close to the second-order one, the coexistence of ferroelectric and paraelectric phases vanishes as the tricritical point is approached from the region of the first-order transition.

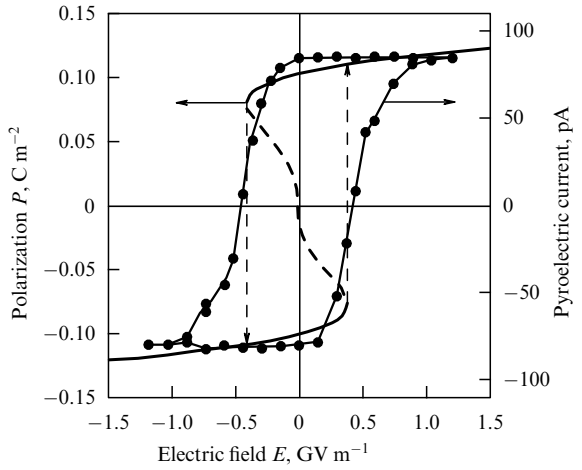


**Figure 1.** Measured hysteresis loop (points) and the theoretical relation $P(E)$ [solid line, from Eqn (2.7)] for a ferroelectric polymer.

Spontaneous polarization may also occur in a crystal as a secondary effect as a consequence of more complicated changes in the crystal structure. In this case, the order parameter of the phase transition is not proportional to the polarization $P$, but to some other parameter, e.g., spontaneous deformation. In other words, the polarization is no longer the driving parameter of the transition, but it may arise or change as a consequence of structural changes. This type of phase transition is called an improper ferroelectric phase transition and the corresponding crystals are called improper ferroelectrics. The typical feature of the improper ferroelectric is a change in the number of atoms in the unit cell volume at phase transition. Improper ferroelectric phase transitions can be modeled by the Landau–Ginzburg theory provided that the free energy expansion includes terms proportional to the true order parameter and cross terms between the order parameter and the polarization [19]. The inorganic oxide, $Gd_2(MoO_4)_3$ [29] and ferroelectric liquid crystals [30] are examples of improper ferroelectrics.

All these thermodynamic results are complicated in real transitions by crystal nonuniformities, defects, grain boundaries, and domains. These complications have little effect on the phase transition but strongly influence polarization hysteresis (switching).

## 3. Thin ferroelectric films and the finite-size effect

The previous discussion did not take into account two important factors with finite samples that necessarily have surfaces, the surface energy and the depolarization energy. The extinction of spontaneous polarization at a surface causes the order parameter $P$ to vary as a function of the distance from the surface $z$ (we consider the one-dimensional uniaxial case). The Landau–Ginzburg free energy density expansion (2.1) must include terms due to the polarization gradient normal to the surface, which imposes a new symmetry condition. The two surface terms are a gradient term in the ferroelectric material proportional to $|\nabla P|^2$ and a polarization discontinuity term proportional to $|\Delta P|^2$ at the surface. The second factor is the depolarization field, which can suppress the phase transition, although this term can be largely compensated by surface charge accumulated through internal or external conductance. The depolarization factor may be important even in the presence of electrodes. In ferroelectric films these two factors are important and lead to the so-called finite-size effect, i.e., to the dependence of the ferroelectric properties on the film thickness.

First, we consider the finite-size effects due to surface energy in the absence of the depolarization field. The review of Tilley [9] summarizes these results, which were obtained in many publications [31–36]. Let us consider a uniaxial ferroelectric film, where the spontaneous polarization $P$ is perpendicular to the film surfaces located at positions $z = \pm L/2$. In the absence of a field ($E = 0$), the Gibbs free energy per unit area has the form [34]

$$G = F_0 + \frac{1}{L}\int_{-L/2}^{L/2}\left[\frac{\alpha}{2}P^2 + \frac{\beta}{4}P^4 + \frac{\gamma}{6}P^6 + \frac{D}{2}\left(\frac{\partial P}{\partial z}\right)^2\right] dz$$
$$+ \frac{D}{2\delta}(P_+^2 + P_-^2) . \tag{3.1}$$

Here, $D$ is the correlation factor, $\delta$ is the decay length determining the strength of coupling in the surface layer, and $P_{\pm}$ are the values of the spontaneous polarization at $z = \pm L/2$. (The material is assumed embedded in a nonpolar medium, so that $\Delta P_{\pm} = P_{\pm}$.) But it is possible for the ferroelectric material to induce polarization into the embedding dielectric, with interesting consequences, as demonstrated in recent papers [37, 38].) The equation of state derived from the generalized free energy (3.1) has the form of the Euler – Lagrange equation:

$$D\,\frac{\partial^2 P}{\partial z^2} = \alpha P(z) + \beta P^3(z) - \gamma P^5(z) - \frac{4\pi}{L}\int_{-L/2}^{L/2} P(z)\,\mathrm{d}z \quad (3.2a)$$

with boundary conditions,

$$\frac{\partial P}{\partial z} \pm \frac{1}{\delta}\,P(z) = 0\,, \qquad z = \pm\frac{L}{2}\,. \quad (3.2b)$$

The finite-size effect can be analyzed by numerically solving for the spatial distribution of the polarization from Eqns (3.2a, b).

If the coupling to the surface polarization discontinuity is positive ($\delta > 0$), there is a decrease in the magnitude of the spontaneous polarization $P$, which is most pronounced at the surfaces ($z = \pm L/2$). The temperature of the phase transition $T_c$ decreases as the film thickness $L$ decreases. Note a very important point that the ferroelectric state of the film does not break into separate bulk and surface states with different transition temperatures, but remains a single state with a single transition temperature $T_c$. The opposite case with negative coupling ($\delta < 0$) leads to an increase in the polarization $P$, most pronounced near the surface, and an increase in $T_c$ with a decrease in the thickness $L$. Figure 2 shows the finite-size effect for positive coupling ($\delta > 0$) on the polarization $P(0)$ in the center of the film (where the polarization is maximum) as a function of the film thickness. Here, $P_b$ is the spontaneous polarization in the bulk material ($L = \infty$) and the thickness $L$ is normalized to the correlation length $\xi = \sqrt{D/|\alpha|}$. The solution shown in Fig. 2, corresponding to the lower value of polarization, is not stable. Figure 2 also shows that the ferroelectric state is completely suppressed in films below the critical thickness

$$L_c \approx 0.85\xi = 0.85\sqrt{\frac{D}{|\alpha|}}\,. \quad (3.3)$$

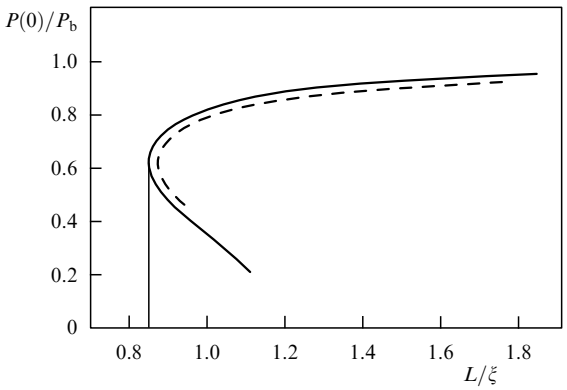


**Figure 2.** Critical thickness in the mean-field theory for positive surface energy, $\delta > 0$ [34].

The parameters $D$ and $\alpha$ are unknown and it is not yet possible to estimate the limiting thickness based on surface energies.

Let us now show the role of the second factor, the influence of the depolarization field on the finite-size effect [9]. The depolarization field will introduce a term to the free energy density (3.1) that will tend to suppress ferroelectricity, increasing the critical thickness $L_c$ and decreasing the polarization $P$ and the transition temperature $T_c$. Consider a ferroelectric film of thickness $L$ covered on both sides by metal electrodes each of thickness $L_e/2$, as shown in Fig. 3. If the electrodes are connected together, charge accumulates within the electrodes to screen the spontaneous polarization of the ferroelectric film. The charge does not completely screen the polarization because the charge must be spread out over a finite Thomas – Fermi screening length $l_s$. Then the screening charge distribution in the electrodes contributes to the generalized free energy (3.1) in the ferroelectric film by an amount

$$\Delta G_s = -\int_{-L/2}^{L/2}\left[\frac{V}{L+L_e}\,P(z) + \frac{1}{2}\,E_d(z)P(z)\right]\mathrm{d}z\,, \quad (3.4a)$$

where $V$ is the voltage applied to the electrodes and $E_d$ is the depolarization field consistent with the Poisson equation (with no free charge inside the ferroelectric film)

$$\frac{\mathrm{d}E_d}{\mathrm{d}z} = -\frac{1}{\chi}\,\frac{\mathrm{d}P}{\mathrm{d}z}\,, \qquad |z| \leqslant \frac{L}{2}\,, \quad (3.4b)$$

where $\chi$ is the polarizability of the ferroelectric from Eqn (2.8). To this, we should add the boundary condition

$$\int_{-(L+L_e)/2}^{(L+L_e)/2} E(z)\,\mathrm{d}z = V \quad (3.4c)$$

and the Thomas – Fermi equation for screening in the electrode†:

$$\frac{\mathrm{d}^2 E}{\mathrm{d}z^2} = \frac{E}{l_s^2}\,, \qquad \frac{L}{2} < |z| < \frac{L+L_e}{2}\,. \quad (3.4d)$$

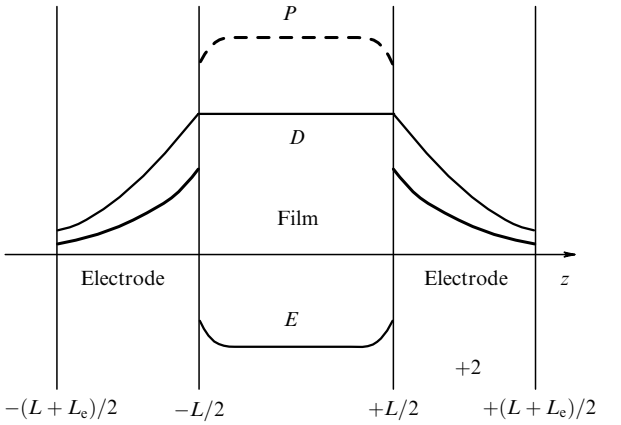


**Figure 3.** Schematic of the depolarization fields for a ferroelectric sample enclosed between metal electrodes [9].

† A similar term can be included in (3.4b) for the charge in the ferroelectric film, present due to conduction or injection, though the screening length is expected to be much larger and therefore the screening much smaller. (*Authors' note for English Edition.*)

The analysis of (3.4) performed by Tilley [9] shows that the depolarization field leads to a renormalization of the Landau – Ginzburg expansion coefficients in (2.1) and therefore to an additional finite-size effect. Tilley calculated the critical thickness of the film as

$$L_c = \frac{2\chi C}{T_{cb}\varepsilon_0} l_s , \tag{3.5}$$

where $T_{cb}$ is the phase transition temperature of the bulk material. Figure 4 shows the dependence of the normalized transition temperature $t = T_c/T_{cb}$ of the finite film on the normalized thickness $x = L/L_c$.

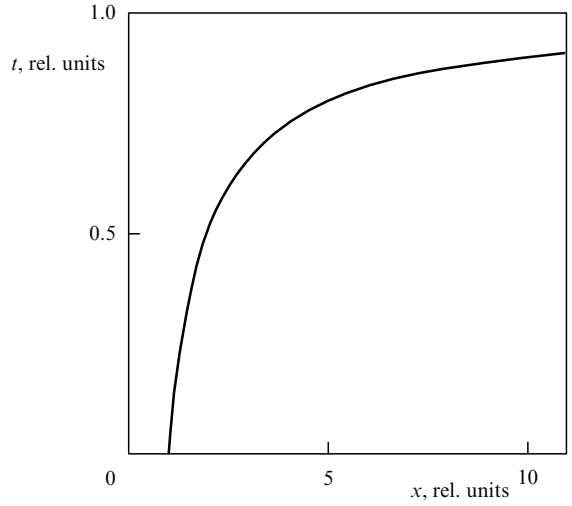


**Figure 4.** Critical thickness obtained in the depolarization model [9].

For Au electrodes, we have $l_s \cong 0.8$ A and the Tilley formula gives for the prototypical displacive ferroelectric barium titanate ($C = 1.8 \times 10^5$ K, $\chi = 134$, $T_{cb} = 403$ K [14]) a critical thickness $L_c \cong 5.3$ A, a thickness not achievable in oxide ferroelectrics. For polyvinylidene fluoride and its copolymers, the critical thickness is $L_c \cong 1$ A, also unachievable.

The finite-size effect in ferroelectric films was analyzed using a transverse Ising model introduced in a general form by de Gennes [39] and applied to ferroelectrics [31, 36]. This model is mainly restricted to ferroelectric transitions involving reforming of hydrogen bonds, as in KDP. The Ising model also describes the dependence of $T_c$ and $P$ on the film thickness and predicts the existence of a critical thickness $L_c$. Since at the surface the interaction between neighboring protons may be changed drastically, the tunneling of protons from one side of the double well to the other disorders the structure and there is no transition to the ferroelectric phase, a limitation that suppresses ferroelectricity in thin films and is the origin of the critical thickness obtained using the three-dimensional Ising model.

Published experimental results demonstrating the finite-size effect are shown in Figs 5a, b. Figure 5 displays the phase diagram showing a slight enhancement of $T_c$ in $KNO_3$ thin films [35]. In thick films, the ferroelectric phase III exists at ambient pressure only between 386 K and 393 K. In thin films (down to 9 μm in thickness) the ferroelectric phase region is greatly broadened. Figure 5b shows the suppression of ferroelectricity, the sharp decrease of $T_c$ in sintered $PbTiO_3$

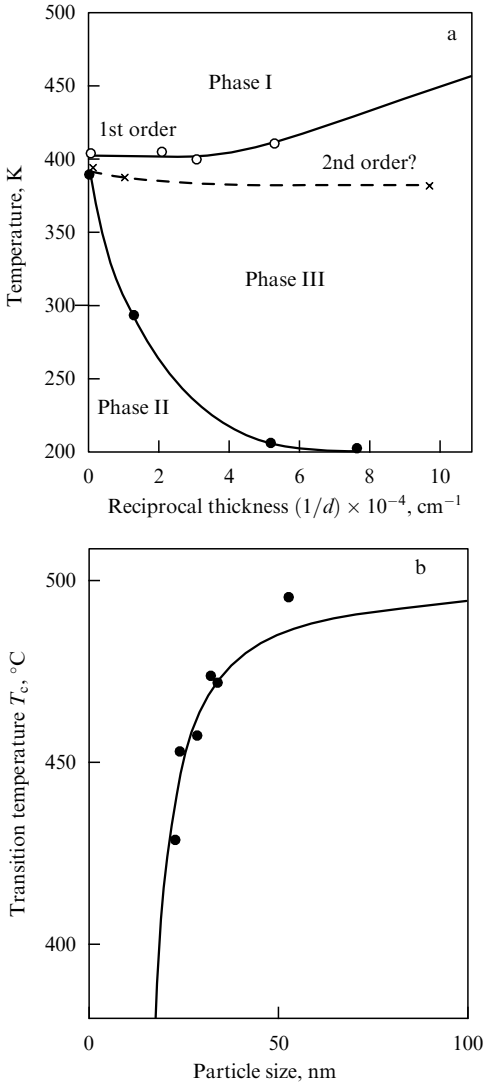


**Figure 5.** (a) Phase diagram for ferroelectric $KNO_3$ thin films, showing the finite-size effect on transition temperatures [35]. (b) The finite-size effect on the transition temperature in sintered $PTiO_3$ crystals [5].

samples as the average size of crystallites approaches a critical size of about 20 nm [5].

## 4. Ferroelectric polymers: vinylidene fluoride copolymers

Here, we briefly review the properties of bulk ferroelectric polymers. These materials have been more completely reviewed by Furukawa [40, 41], by Lovinger [42, 43], and in the books edited by Wang, Herbert, and Glass [44] and by Nalwa [45].

Ferroelectric polymers are of great scientific interest, yielding a wealth of physical data [41], while the rapid commercialization of piezoelectric transducers made from these materials is a model of technology transfer [44, 46]. Ferroelectric polymer films can serve many of the functions presently or potentially filled by traditional inorganic ferroelectric materials [44]. Ferroelectricity was established first in polyvinylidene fluoride, PVDF [47], and then its copolymers with trifluoroethylene P(VDF – TrFE) [48] and tetrafluoroethylene P(VDF – TeFE) [49]. Ferroelectric P(VDF – TrFE)

exhibits many properties characteristic of ferroelectric and noncentrosymmetric materials, including pyroelectric and piezoelectric effects [41], bulk photovoltaic (photogalvanic) currents [50], electrooptic modulation [51], second harmonic generation [52], and possible photorefractive effects [53]. Other known ferroelectric polymers include nylon-11 [54], and other odd-numbered nylons [55]. There are also a number of liquid-crystal ferroelectric polymers with applications in display technology [56].

Ferroelectric polymers are a rich system for the study of phase transitions and ferroelectricity; they exhibit all the interesting physical phenomena we associate with inorganic ferroelectrics like barium titanate and yet exhibit fundamentally different microscopic interactions, dominated by hydrogen bonding and van der Waals forces. They have the potential to replace inorganic ferroelectrics in many applications and offer some unique applications of their own. Ferroelectric polymer films have, until recently, been fabricated by solvent casting or, better, by solvent spin coating [48], a method that yields polydomain films with up to 85 % crystallinity [44, 57]. Ferroelectric polymers formed by spinning, casting and other bulk techniques are polymorphous, containing amorphous material and crystalline phases. Films must be textured mechanically and electrically to achieve macroscopic piezoelectric behavior, though they still contain amorphous material and the crystallites are incompletely oriented [41, 44]. The properties of the solvent-formed films strongly depend on the crystallinity and morphology, and these factors suffer from significant thermal instability when cycled through the transition and melting temperatures.

PVDF, the prototypical ferroelectric polymer, is a linear fluorinated hydrocarbon with a repeat unit ($CH_2-CF_2$) of spacing 2.6 A, as shown in Fig. 6a. The PVDF chains have a net dipole moment, pointing from the electronegative fluorine to the electropositive hydrogen, producing a net dipole moment nearly perpendicular to the polymer chain. These chains can crystallize in a quasi-hexagonal close-packed '$\beta$-phase' structure with the dipoles of all chains aligned in a structure with maximum polarization $P \cong 0.13\,\mathrm{C\,m^{-2}}$. Poling and switching are accomplished by applying a large electric field perpendicular to the chains to reverse the direction of polarization.

However, the temperature of the paraelectric – ferroelectric phase transition in PVDF is above its melting temperature. Therefore, most studies of ferroelectric properties were conducted on the copolymers P(VDF – TrFE), random copolymers of vinylidene fluoride and trifluoroethylene monomers with structure $(CH_2-CF_2)_n-(CHF-CF_2)_m$. The copolymers with 50% or less TrFE are ferroelectric, though with reduced polarization and transition temperatures, because some of the hydrogen atoms are replaced with fluorine, reducing the net dipole moment of the polymer chains [58]. Spun polymeric films reveal rapid (about 1 μs) ferroelectric switching, which depends on the electric field and film thickness [41].

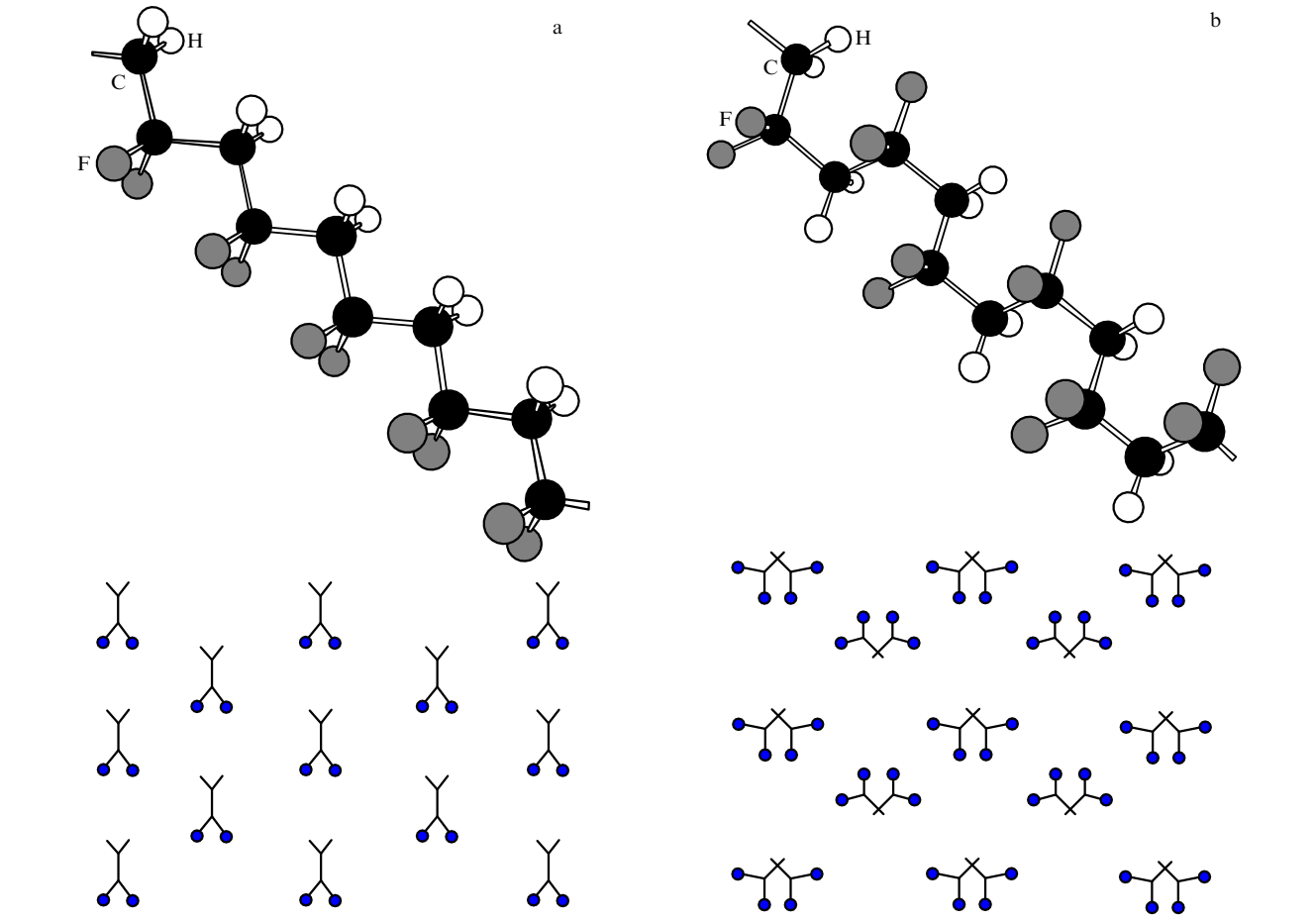


**Figure 6.** (a) Diagram of PVDF in the all-trans conformation. (b) Diagram of PVDF in the alternating-gauche conformation.

The most studied copolymers have a composition near 70% VDF. The P(VDF–TrFE 70:30) copolymer has a maximum spontaneous polarization $P \cong 0.1$ C m$^{-2}$, a first-order ferroelectric–paraelectric phase transition at $T_c \cong +100\,^{\circ}$C and large temperature hysteresis. In the phase transition, the structure changes from the all-trans (TTTT) configuration arranged in a dipole-aligned structure (Fig. 6a) to the alternating trans-gauche (TGTG) configuration arranged in a nonpolar structure (Fig. 6b). The copolymers also have a slightly larger unit cell than pure PVDF owing to the replacement of some of the hydrogen atoms on one side of the chains by the larger fluorine atoms.

The finite-size effect has been demonstrated in films of the P(VDF–TrFE 75:25) copolymer formed by solvent spinning. Films as thin as 600 A studied by Kimura [7] show an increase in the coercive field with decreasing thickness (Fig. 7). Solvent methods like spinning have been unable to make good films thinner than 600 A, so further study of the finite-size effect was not done for nearly ten years following Kimura's work.

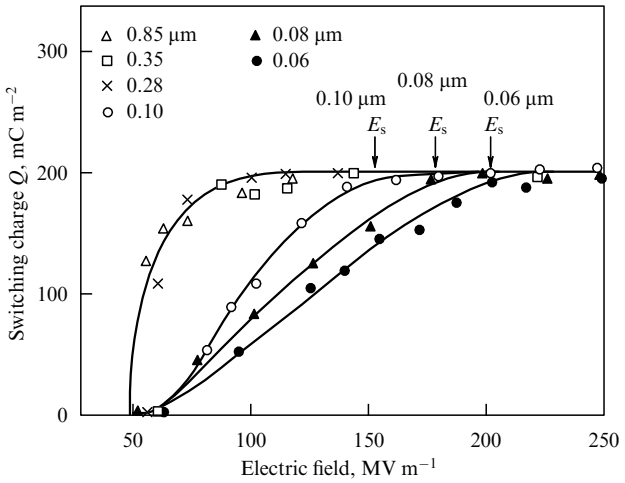


**Figure 7.** Dependence of switching charge (polarization reversal) in the P(VDF–TrFE, 75:25) copolymer on the external electric field for copolymer films with different thicknesses [7].

However, in 1995 we developed very-high-quality crystalline oriented films of the copolymer P(VDF–TrFE) formed by Langmuir–Blodgett (LB) deposition and confirmed that the films have the key ferroelectric properties, including switching and the ferroelectric phase transition of the first order [59, 60]. As was mentioned in the introduction, the LB technique permitted us for the first time to prepare ultrathin ferroelectric films as thin as one monolayer (ML), 5 A, thus allowing the study of the finite-size effect on a scale never before investigated in ferroelectric materials. These results are reviewed in the next section.

## 5. Langmuir–Blodgett ferroelectric films

LB films are well-known structures prepared as a result of successive transfer of monolayers from the gas–liquid interface onto solid substrates. One impressive possibility of the LB method is the opportunity to vary the multilayer structure of LB films to an accuracy of one monolayer, when the kind of molecules as well as their orientation in a single monolayer can be controlled [61–63].

High-quality thin films of ferroelectric P(VDF–TrFE 70:30) were fabricated by the horizontal Schaefer variation of the Langmuir–Blodgett monolayer transfer technique, shown in Fig. 8a, permitting precise control of the film nanostructure [59, 64]. The ferroelectric LB films were prepared from a P(VDF–TrFE 70:30) copolymer solution in dimethyl-sulfoxide of concentration 0.01 wt.% [59]. This solution was dispersed on a triple-distilled water subphase in a home-built LB trough, and the pressure–area isotherms (Fig. 8b) were measured to identify the conditions forming closest packing of a film of monolayer thickness. At room temperature, these conditions were satisfied at a surface pressure of 5 mN m$^{-1}$ and an area of 5.7 A$^2$ per molecule [59]. (Films formed at significantly higher surface pressures buckle and fold, producing poor samples [65].) The films for electric measurements were deposited on aluminum-coated glass or silicon substrates and overcoated with aluminum evaporated in a vacuum. Films for STM measurements were deposited on cleaved pyrolytic graphite, and films for X-ray, neutron, and electron diffraction studies were deposited on silicon substrates of different orientations. Film preparation is described in greater detail elsewhere [59, 61, 66].

The structure and uniformity of the films were checked by means of atomic-resolution tunneling microscopy [67–69], X-ray and neutron diffraction [70, 71], low-energy electron diffraction (LEED) [69], and scanning electron microscopy.

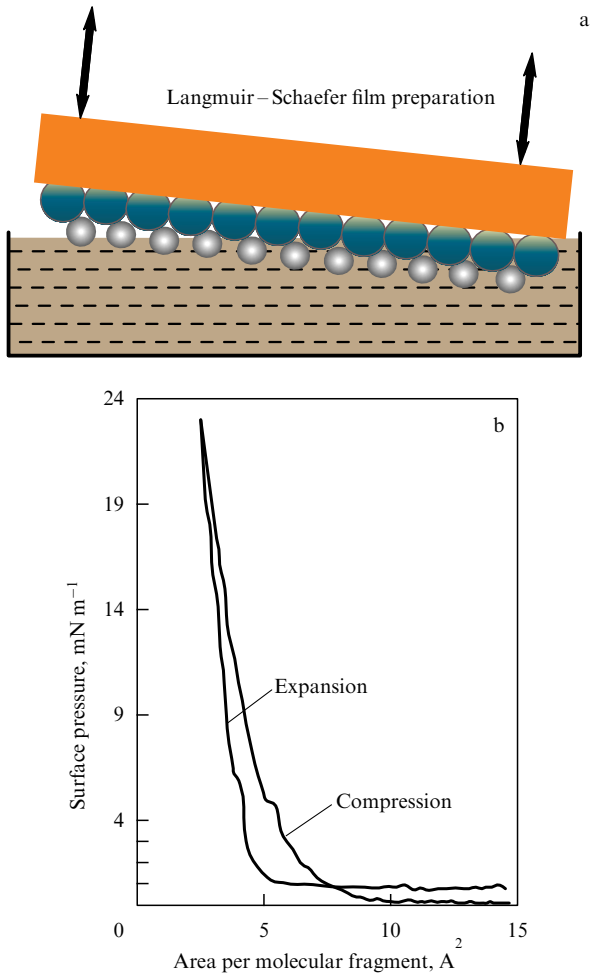


**Figure 8.** (a) Diagram of the Langmuir–Schaefer monolayer deposition method. (b) Pressure–area isotherm of P(VDF–TrFE 70:30) [59].

The ferroelectric LB films apparently have a very high crystallinity and are highly oriented with the polarization axis perpendicular to the film plane; yet, we presume the films are polycrystalline with randomly oriented regions of parallel-chain crystals. The ferroelectric LB films have an unmistakable first-order bulk ferroelectric phase transition as demonstrated by clear thermal hysteresis of the dielectric constant [59, 60], complete reversible polarization switching below $T_c = 80\,^\circ$ [60, 67], and by the observation of double hysteresis between $T_c$ and a ferroelectric critical point at 145 °C [72].

Atomic-resolution scanning tunneling microscopy (STM) images show that the films can have excellent crystalline structure with the polymer chains aligned parallel to each other in the plane of the film as shown in Fig. 9 [68]. Although all images show excellent ordering along the chains — this is expected as the covalent bonds rigidly hold the 2.6 A spacing between monomers — some of the images, like the one in Fig. 10a, show some disorder in the interchain spacing, which ranges from 3.5 A to 4.3 A in this image. The Fourier transform of this STM image (Fig. 10b) and the LEED image (Fig. 10c) both have a series of evenly spaced lines. These lines are perpendicular to the direction of the polymer chains and confirm the excellent order along the chains. But the lines also reveal disorder perpendicular to the chains. The LEED pattern (Fig. 10c) further reveals weak bright spots along the lines consistent with some long-range order in the direction perpendicular to the chains. It must be stressed that, unlike the spun films, the LB films do not contain an amorphous phase and, therefore, are more stable. Nevertheless, annealing of LB films influences their crystallinity and physical properties. After a few annealings the properties become quite stable. It is possible to suppose that annealing stabilizes the equilibrium structure of the crystal by ordering the interchain separation.

Both X-ray [71] and neutron [70] diffraction studies show excellent ordering in the direction perpendicular to the film, along the [010] direction, with layer spacing 4.5 A, in agreement with studies of bulk films [73]. Figure 11 shows representative diffraction peaks recorded at room temperature using a $\theta - 2\theta$ geometry. Analysis of the X-ray data shows that the structural coherence length in the direction perpendicular to the film is about 300 A. The X-ray studies were carried out in films as thin as 5 ML (25 A thick) and 150 ML (750 A thick). Figure 12 shows the thermal hysteresis in the layer spacing (or the period $b$) in a 5-ML film (Fig. 12a) and a 150-ML film (Fig. 12b) [71]. This hysteresis, also observed by Legrand in bulk films [73], is a consequence of the metastable coexistence of the ferroelectric phase (4.5 A, see Fig. 6a) and the paraelectric phase (4.6 – 4.9 A, see Fig. 6b) upon the first-order phase transition. The similarities between the thinner and thicker films across the bulk (80 °C) phase transition confirms that the thin films share a common bulk ferroelectric phase with the thicker films.

The presence of the ferroelectric – paraelectric phase transition is also confirmed by dielectric measurements [59, 60, 67, 74, 75]. The transition is revealed by the dielectric anomalies shown in Fig. 13a [59, 60, 72] and the peak in the pyroelectric response shown in Fig. 13b [68, 76]. The thermal hysteresis and phase coexistence are also evident from the dielectric measurements shown in Fig. 13a where the dielectric peak of a 30-monolayer film (measured at zero electric field, solid line in Fig. 13a) appears at about 113 °C on heating and at 75 °C on cooling. This temperature range is in reasonable agreement with the phase coexistence observed in the X-ray diffraction measurements shown in Fig. 12.

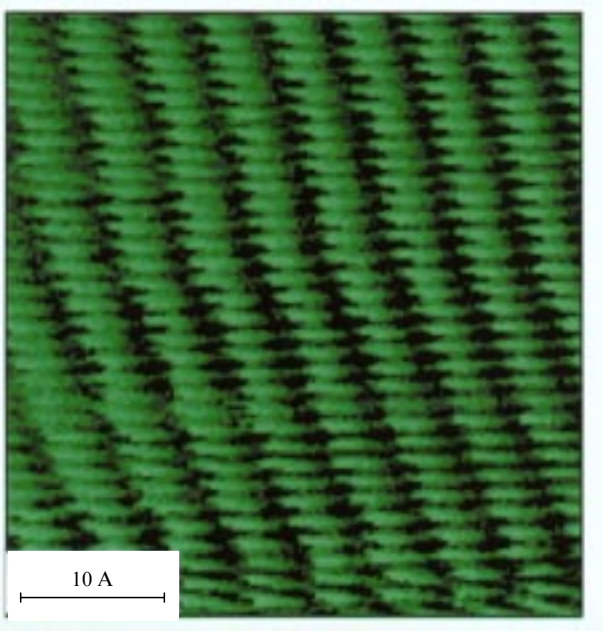


**Figure 9.** STM image of one LB monolayer of the P(VDF – TrFE 70 : 30) copolymer on a graphite substrate [68].

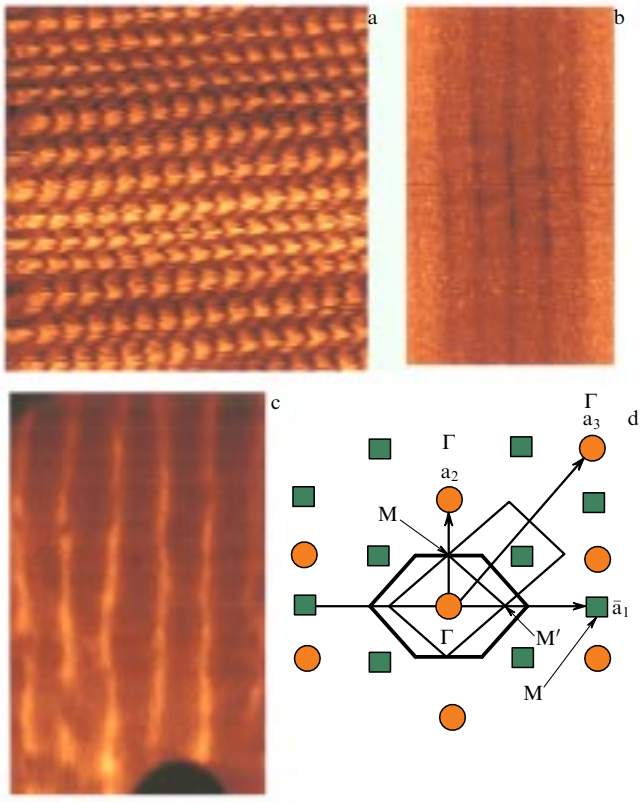


**Figure 10.** (a) STM image of a 2-ML film of P(VDF – TrFE 70 : 30) on graphite. (b) Fourier transform of the STM image shown in (a). (c) LEED image of a 5-ML film of P(VDF – TrFE 70 : 30) on Si (100). (d) Surface Brillouin zone of a 5-ML film of P(VDF – TrFE 70 : 30) on Si (100) [69].

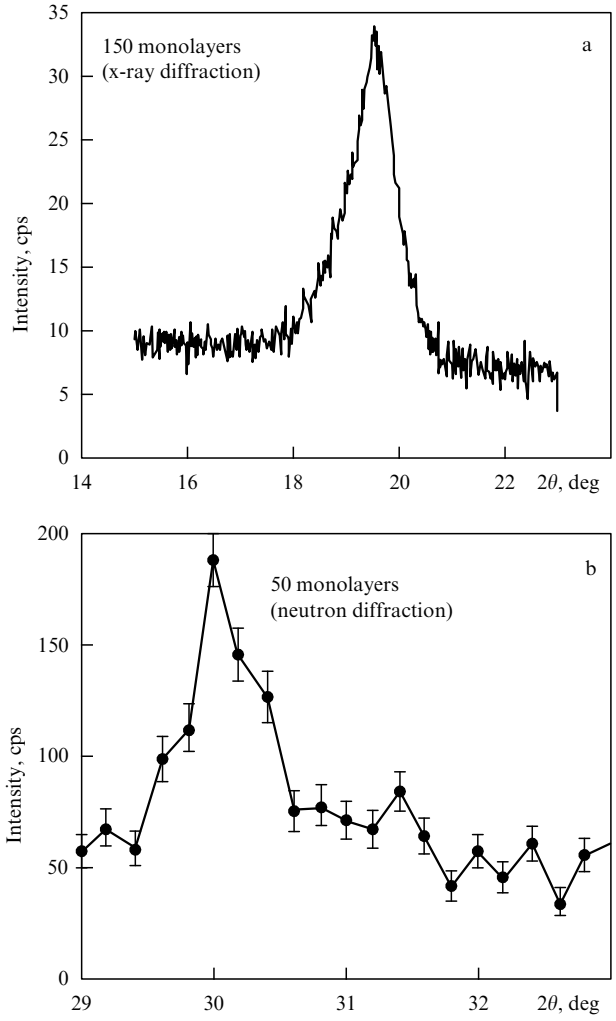


**Figure 11.** (a) X-ray diffraction peak from the $\theta - 2\theta$ measurement of a 150-ML P(VDF – TrFE 70 : 30) film on Si [71]. (b) neutron diffraction peak from the $\theta - 2\theta$ measurement of a 50-ML P(VDF – TrFE 70 : 30) film on Si [70]. The scattering vector is perpendicular to the film plane.

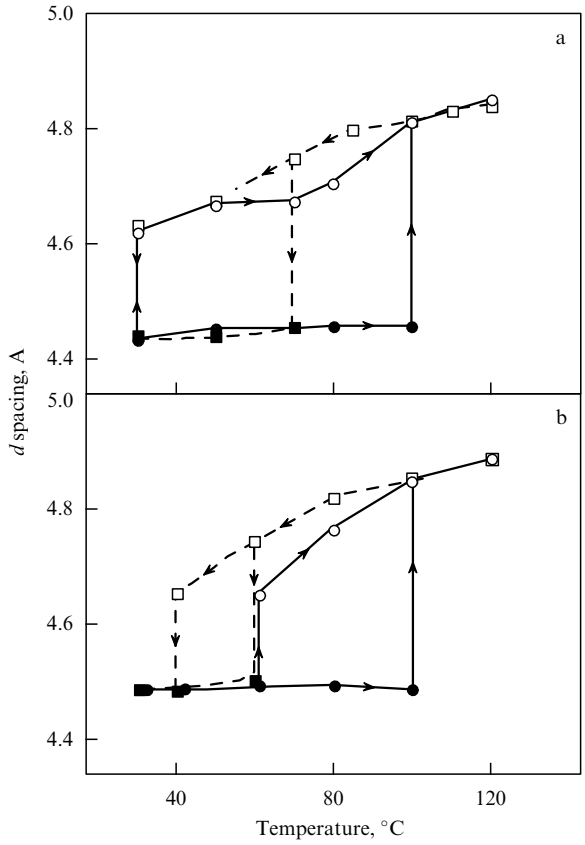


**Figure 12.** Thermal hysteresis of the layer spacing of P(VDF – TrFE 70 : 30) LB films: (a) 5 ML film and (b) 150 ML film [71].

The first-order ferroelectric phase transition temperature $T_c(E)$ can be raised above the zero-field Curie temperature $T_{c0}$ by application of an external electric field. This is demonstrated in the ferroelectric copolymer by the dashed curve in Fig. 13a. Above the critical temperature $T_{cr}$, the ferroelectric phase can no longer be sustained even by very high applied field. The existence of this ferroelectric critical point $(E_{cr}, T_{cr})$ in the electric field – temperature $(E-T)$ phase diagram was predicted by Ginzburg [20, 21] and Devonshire [13, 25, 26] using the Landau mean-field theory of phase transitions. The shift of $T_c$ with the electric field and the presence of a critical point have been clearly demonstrated in $BaTiO_3$ [77] and KDP ($KH_2PO_4$) [78, 79], both proper ferroelectrics with first-order phase transitions, and also in a ferroelectric liquid crystal [30], a first-order improper ferroelectric in which the order parameter is the molecular tilt, not electric polarization.

The 'butterfly' capacitance $C(E) \cong dP/dE$ curves shown in Fig. 14a for the first time demonstrate double hysteresis and identify the ferroelectric critical point in a ferroelectric polymer — conclusive evidence that this is a first-order ferroelectric phase transition [72]. Below the zero-field ferroelectric phase transition temperature $T_{c0} = +80 \pm 10\,^{\circ}C$, there is one hysteresis loop centered at zero field, giving two peaks in capacitance at the coercive field $E_c(T)$, one on each side of the zero bias. Above the zero-field ferroelectric phase transition $T_{c0}$ but below the critical temperature $T_{cr} \approx +145 \pm 5\,^{\circ}C$, there are four peaks in the capacitance due to two hysteresis loops arranged antisymmetrically about the zero bias [77]. The dual hysteresis loops occur because the sample is not ferroelectric at zero field but the ferroelectric state is induced at sufficiently high field. There is no hysteresis observed at 150 °C (Fig. 14) and, therefore, the temperature is above the ferroelectric critical temperature $T_{cr}$. The 'butterfly' curves in Fig. 14 permit us to construct the $E-T$ phase diagram at atmospheric pressure (Fig. 15). The electric field at the boundary between the ferroelectric and paraelectric phases is the center of the hysteresis loop, or the midpoint between the pairs of peaks at both positive and negative bias. Since we observed double hysteresis at 140 °C and not at 150 °C, the critical point is contained within the ellipse centered at $T_{cr} \approx +145 \pm 5\,^{\circ}C$ and $E_{cr} \approx 0.93 \pm 0.1$ GV m$^{-1}$. Table 1 gives values of $dT_c/dE$, $E_{cr}$, $T_{cr}$ for P(VDF – TrFE 70 : 30) as well as for $BaTiO_3$, KDP, and a ferroelectric liquid crystal. Ferroelectric polymers have a relatively large range of field-induced phase transition temperatures $T_{cr} - T_{co} = 65 \pm 11\,^{\circ}C$ as compared to other ferroelectric materials like $BaTiO_3$ [14, 77], KDP [78, 79], and ferroelectric liquid crystals [30] because of the relatively weak van der Waals interaction in the polymers [41].

The piezoelectric and pyroelectric effects are well established in PVDF [52, 80] and its copolymers. However, there is still uncertainty about the mechanism and the contributions

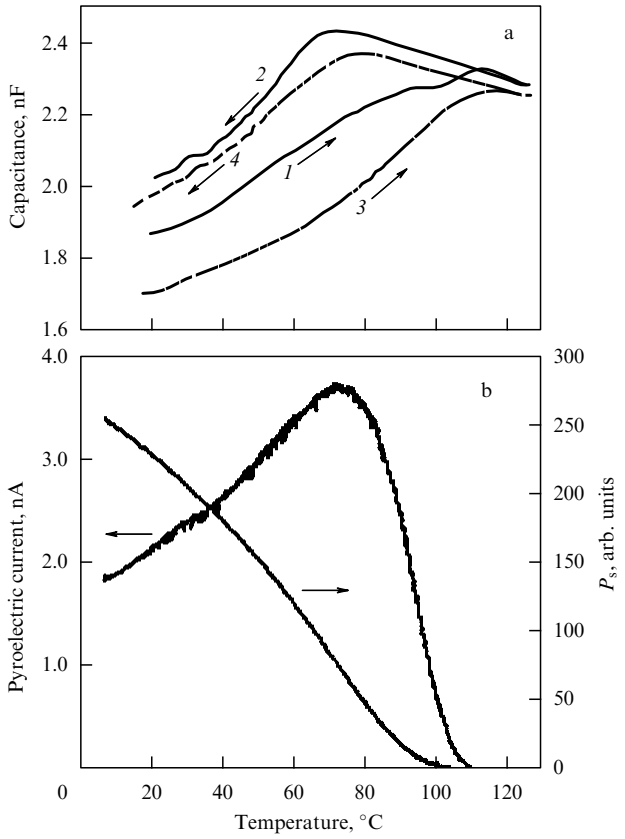


**Figure 13.** (a) Temperature dependence of the capacitance at zero bias voltage (curves *1* and *2*) and under a bias voltage of 5 V (curves *3* and *4*) in a 30-ML film of P(VDF – TrFE 70 : 30) [72]. (b) Temperature dependence of the pyroelectric response of a 30-ML film of P(VDF – TrFE 70 : 30) measured by the Chynoweth method [76].

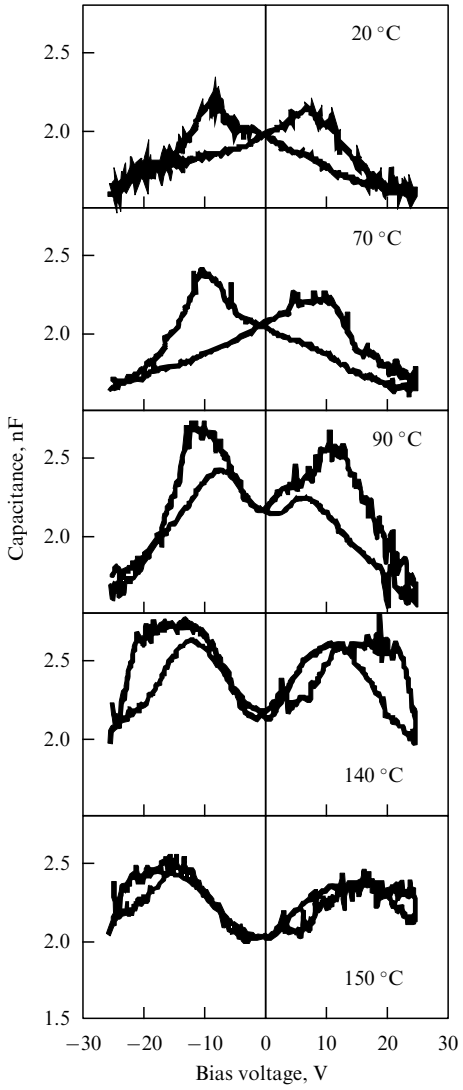


**Figure 14.** 'Butterfly' capacitance hysteresis curves of a 30-ML film of P(VDF – TrFE 70 : 30) at temperatures spanning both the Curie point $T_c = 80 \pm 10\,^{\circ}\mathrm{C}$ and the critical point $T_{cr} = 145 \pm 5\,^{\circ}\mathrm{C}$. The field was ramped at 0.02 V $s^{-1}$ during measurements [72].

from the amorphous phases and polycrystals in typical bulk films formed by solvent techniques [81 – 83].

The piezoelectric and pyroelectric coefficients of P(VDF – TrFE 70 : 30) 30-monolayer thick LB films were measured by interferometric and thermal modulation methods described in detail earlier [76]. The coefficients of the piezoelectric tensor are defined by [84]

$$d_{kij}^{\tau} = \left[\frac{\partial S_{ij}}{\partial E_k}\right]_{\tau}, \qquad (5.1)$$

where $S_{ij}$ is the strain tensor, $E_k$ is the electric field, and $\tau$ denotes that the measurements are made at constant stress (low frequency). We measured the effective piezoelectric coefficient $d_{333}^{\mathrm{eff}}$, where the '3' direction is perpendicular to the film [76]. The temperature dependence of the spontaneous polarization was calculated by integrating the pyroelectric coefficient over temperature (Fig. 13b). Similarly, the coefficients of the pyroelectric tensor are defined by [84]

$$p_i^{\tau} = \left[\frac{\partial P_i}{\partial T}\right]_{\tau}, \qquad (5.2)$$

where $P_i$ is the spontaneous polarization. We measured the effective pyroelectric coefficient $p_3^{\mathrm{eff}}$ [76]. A comparison of the piezoelectric and the pyroelectric coefficients in LB films and spun films (Table 2) shows good agreement.

Both piezoelectric and pyroelectric responses along the polarization axis at a given temperature are proportional to

**Table 1.** Ferroelectric phase transition parameters for P(VDF – TrFE 70 : 30) films made by Langmuir – Blodgett deposition and solvent spinning, and for potassium dihydrogen phosphate (KDP), barium titanate ($BaTiO_3$), and a ferroelectric liquid crystal (FLC).

| Material | $T_{c0}$, °C | $T_{cr}$, °C | $E_{cr}$, V $m^{-1}$ | $dT_c/dE$, mK $V^{-1}$ |
|---|---|---|---|---|
| LB polymer | $+80 \pm 10$ | $+145 \pm 5$ | $(0.93 \pm 0.1) \times 10^9$ | $(7.0 \pm 2) \times 10^{-8}$ |
| Spun polymer [41] | +102 | No data | No data | $12 \times 10^{-8}$ |
| $BaTiO_3$ [77] | +108 | +116 | $0.6 \times 10^6$ | $6.5 \times 10^{-4}$ |
| KDP [78, 79] | −61 | −60 | $0.83 \times 10^6$ | $1.25 \times 10^{-6}$ |
| FLC [30] | +55.0 | +55.8 | $5.0 \times 10^6$ | $1.6 \times 10^{-7}$ |

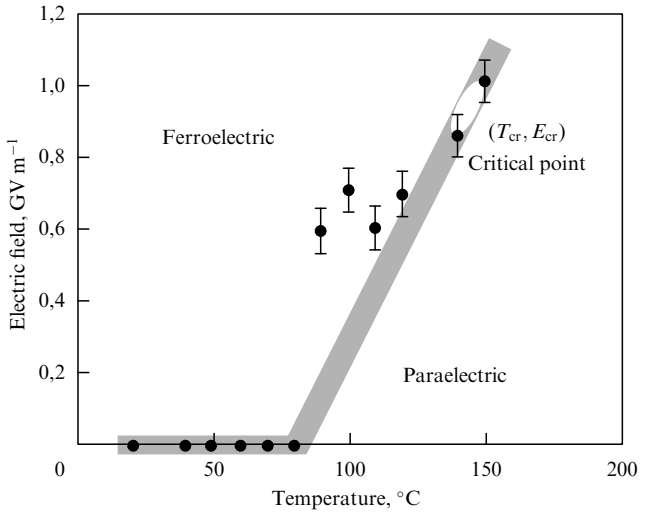


**Figure 15.** Ferroelectric $E-T$ phase diagram of a 30-monolayer LB film of P(VDF – TrFE 70 : 30) at atmospheric pressure showing the zero-field phase transition temperature $T_c = 80 \pm 10\,^{\circ}C$ and the ferroelectric critical point $T_{cr} = 145 \pm 5\,^{\circ}C$. The data points were derived from 'butterfly' hysteresis curves like those shown in Fig. 14 [72].

**Table 2.** Comparison of the piezoelectric and the pyroelectric coefficients of LB films (30 ML) and spun films.

| Material | $d_{33}$, $10^{-9}$ m V$^{-1}$ | $p_3$, μC m$^{-2}$ K$^{-1}$ | $P_s$, C m$^{-2}$ |
|---|---|---|---|
| LB film | $20 \pm 2$ [76] | $20 \pm 4$ [76] | 0.1 [76] |
| Spun film | 40 [83] | 35 [97] | 0.1 [41] |

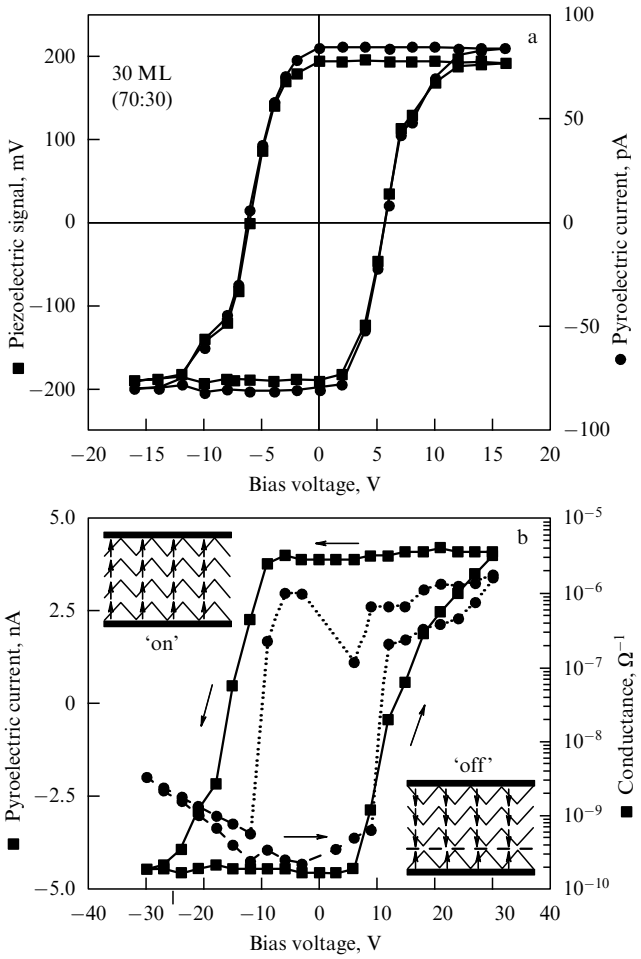


**Figure 16.** (a) Hysteresis loop of the effective piezoelectric coefficient $d_{33}$ and pyroelectric response of a 30-ML film of P(VDF – TrFE 70 : 30) [76]. (b) Hysteresis in the pyroelectric current (squares) and in the conductance (solid circles) of a 30-ML film of P(VDF – TrFE 70 : 30). Insets: orientation of the polymer chains in the ON state of the fully ordered ferroelectric LB film (upper) and in the OFF state of the partially ordered LB film (lower) [60].

the polarization. This is clearly shown in the hysteresis curves in Fig. 16a of the pyroelectric and piezoelectric signals as a function of the bias voltage. The pyroelectric measurements were also used in conjunction with measurements of the switched charge to measure the spontaneous polarization $P_s \approx 0.1$ C m$^{-2}$ at 25 °C and, by integration of the relative pyroelectric response (Fig. 13b), at other temperatures as well.

We have observed a novel conductance switching phenomenon not observed before in ferroelectric materials [60] †. Figure 16b shows that the conductance of the LB film switches from low to high and back to low in coincidence with the polarization switching. The conductance change is three orders of magnitude, a remarkable contrast for a completely nonvolatile and reversible switch. It appears that the conductance switching is controlled by the polarization state, a hypothesis also consistent with the switching dynamics.

The new conductance switching mechanism seems to be connected with the barrier produced by a single polar layer pinned by the substrate or top electrode. Three observations substantially support this hypothesis [60]:

(1) The switching-OFF process is much faster than the bulk polarization reversal, because when the film is in the ON state the reversal of the first layer presents a barrier and switches the conductance OFF.

(2) When the film is switched ON, there is a delay until nearly all the bulk polarization of the film is switched; the transition from low conductance (OFF) to high conductance (ON) occurs only as the polarization of the *last* monolayer switches. The OFF state is maintained because one or a few layers are pinned to the substrate or to the top electrode.

(3) The as-grown films are always partially polarized in the direction of the ON state. This hypothesis is supported by the observation of asymmetric (biased) hysteresis loops in films thinner than 20 layers [74]. The cause of pinning is unknown.

The large conductance in the ON state is consistent with a tunneling current as in the Fowler – Nordheim mechanism [85] observed in other thin organic films [86]. It is also possible that the ON state is dominated by thermally activated hopping mechanism of conduction, with an exponential temperature dependence. In the OFF state, the negative charge sheet at the polarization discontinuity presents a barrier to electron tunneling (or thermally activated hopping). The electrodes also may play an important role (besides the physical pinning of the adjacent layers) in the conductance switching due to carrier injection. However, we observed ferroelectric and conductance switching with several different materials composing the top and bottom electrodes; this suggests that the conductance switching is probably con-

† Recent results from strontium titanate films seem to have the same behavior, see Abe K et al. *Jpn. J. Appl. Phys.* **36** 5846 (1997) (*Authors' note for English Edition*.)

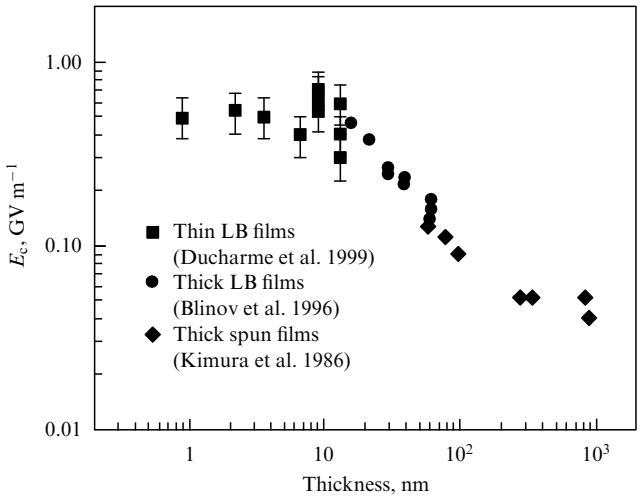


**Figure 17.** Thickness dependence of the coercive field for spun and LB films of the ferroelectric copolymer P(VDF – TrFE) [7, 90].

trolled by an interlayer barrier. Similar conductance switching has recently been observed in PZT thin films [87].

The switching data reported above were all collected at very low frequency, less than 0.01 Hz, because most of the LB ferroelectric polymer films switch very slowly. This is in contrast to bulk films, which can switch in nanoseconds [88] and show an exponential field dependence associated with nucleation-limited switching [41, 89]. With some of our films we observed switching times in the range 1 – 500 μs, but these investigations are still in progress.

Like spun films (see Fig. 7) [7], the ferroelectric LB films of P(VDF – TrFE) show the finite-size effect. In the interval of 30 to 150 ML (∼15 to 75 nm) the decrease in the thickness of the LB film leads to some decrease in $T_c$ and the dielectric constant. The coercive field $E_c$ shows a much larger finite-size effect as shown in Fig. 17. The data from spun films (diamond symbols [7]) and LB films at least 15 nm thick (circle symbols [74]) match very well and show power-law finite size scaling as the thickness to the −0.7 power. But LB films thinner than 15 nm show no finite-size effect; the coercive field $E_c$ is independent of thickness below 15 nm. This also illustrates the two-dimensional nature of the ferroelectric polymer films, as will be discussed in the next section.

## 6. Two-dimensional ferroelectric films

LB technology now permits us not only to investigate the finite-size effect in ferroelectrics on the new scale, but to check the theoretically predicted existence of the critical thickness $L_c$ (see Section 3). We were able for the first time to investigate the ultimate limits of the finite-size effect for P(VDF – TrFE 70 : 30) LB films ranging in thickness from 2 to 30 ML (1 – 15 nm) [68]. Measurements of the dielectric constant, pyroelectric response, and polarization hysteresis all demonstrated the essential two-dimensional character of the ferroelectric state in these films.

Figure 18a shows that multilayer ferroelectric LB films have dielectric anomalies with a large thermal hysteresis, which mark the usual bulk first-order ferroelectric phase transition found at 77 °C on cooling (108 °C on heating) in the 30-ML film, and at 68 °C on cooling (98 °C on heating) in the 2-ML film. Figure 19 shows a very weak dependence of the phase transition temperature $T_c$ on the number of monolayers. The pyroelectric response shown in Fig. 18b also records the bulk transition near 73 °C, though the precise transition temperature is not as clear as in the dielectric

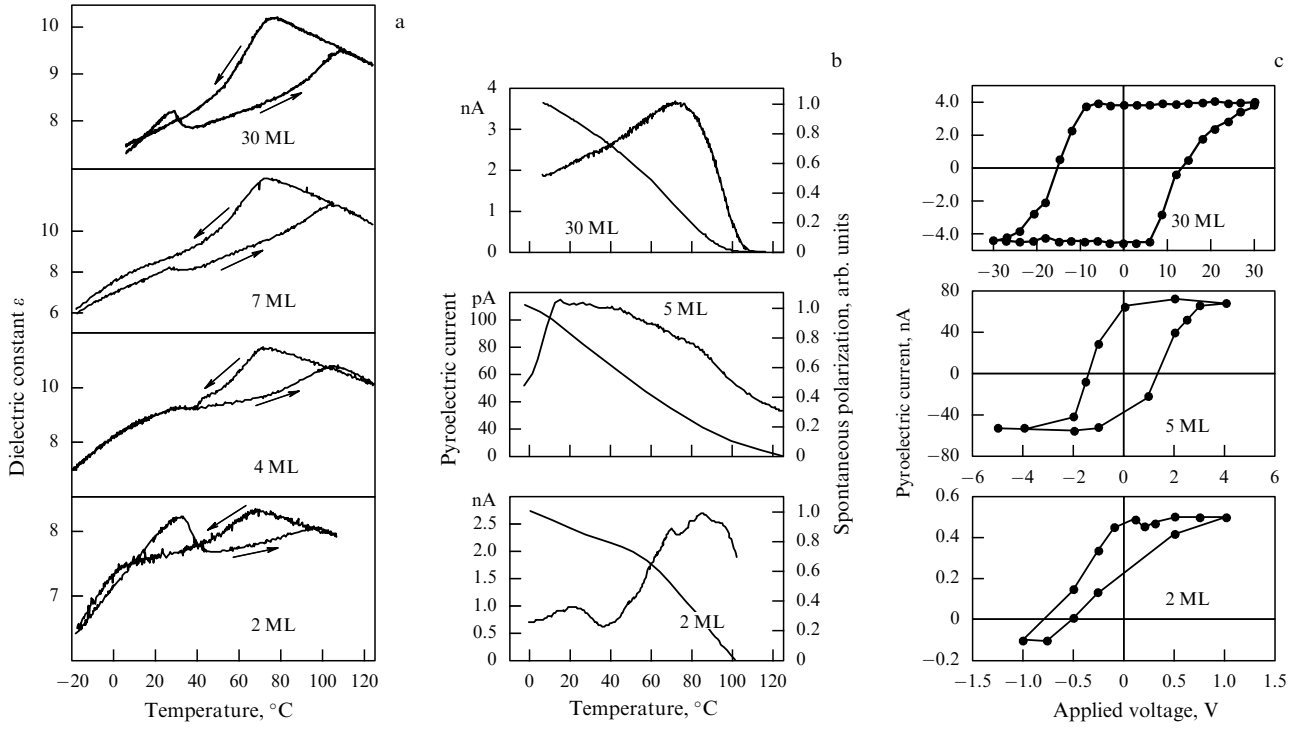


**Figure 18.** (a) Temperature dependence of the dielectric constant in films of P(VDF – TrFE 70 : 30) [68]. (b) Pyroelectric response and spontaneous polarization, obtained by integrating over temperature from films of P(VDF – TrFE 70 : 30) [68]. (c) Polarization hysteresis loops at 25 °C, measured by the pyroelectric technique in LB films of P(VDF – TrFE 70 : 30) [68].

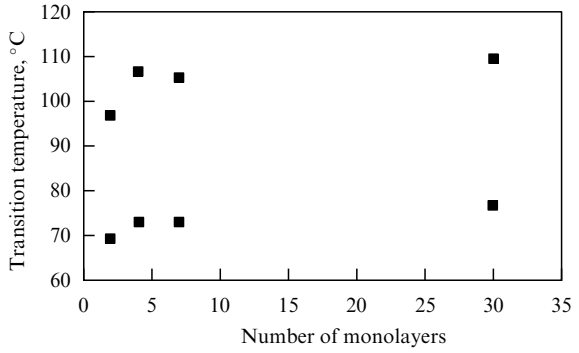


**Figure 19.** Dependence of the ferroelectric–paraelectric transition temperature of P(VDF–TrFE 70 : 30) on the film thickness [68].

measurements. Thus, the 'bulk' first-order phase transition at $\sim 80\,^{\circ}$C remains even in the 2-ML films — a result that challenges the theoretical predictions discussed above that three-dimensional ferroelectricity must vanish in films below a minimum critical thickness.

The hysteresis loops shown in Fig. 18c show good saturation for the 5-ML and 30-ML films and incomplete saturation for the 2-ML film. The 5-ML and 2-ML films show considerable vertical shift, probably due to interactions with the substrate or the top electrode, consistent with the earlier observations on the dynamics of switching in LB films (see Fig. 16 [60, 74]). The films achieved at least 50% of the maximum expected polarization if all dipoles were aligned perpendicular to the film.

Figures 18a and 18b also show a new and unexpected phase transition at a lower temperature of $\sim 20\,^{\circ}$C in films of 30 ML or less. The dielectric constant shows peaks at $\sim 20\,^{\circ}$C on cooling and at 28 °C on heating. There is also a peak in the pyroelectric response. The polarization hysteresis loops from 30-, 5- and 2-ML films (Fig. 18c) show that ferroelectric switching is obtained at 25 °C in all the films, even in as thin ones as 2 ML. In Ref. [68] the behavior at $\sim 20\,^{\circ}$C was attributed to a new first-order ferroelectric transition in the surface layer on the basis of several observations, e.g., the new transition is strongest in the thinnest films; there is clear thermal hysteresis in the dielectric constant; and there are peaks in both the dielectric constant and the pyroelectric response. There is other evidence of the surface nature of this first-order phase transition, which will be discussed later.

One of the striking features of the dielectric properties of the thinnest ferroelectric LB films in the thickness interval of 2–30 ML is the absence of the finite-size effect and very large coercive fields ($0.9 \pm 0.2$ GV m$^{-1}$ for films of 30–2 ML), far larger than in other ferroelectric materials and closely approaching the intrinsic coercive field expected in the absence of nucleation ($\sim 1$ GV m$^{-1}$). Figure 17 shows that in this interval the coercive field $E_c$ does not depend on the film thickness and approaches the intrinsic Landau–Ginzburg value (0.5 GV m$^{-1}$ at $T_0$). This means that the switching of these LB films essentially does not depend on the nucleation and domain kinetics (see Section 2). Let us consider the intrinsic coercive field in more detail.

The intrinsic coercive field is calculated from the extrema of Eqn (2.7) [90]:

$$E_c = \frac{P_0}{\chi_0} f(t), \tag{6.1}$$

$$f(t) \cong \frac{3}{25}\sqrt{\frac{3}{5}}\left[1 - \frac{25}{24}t\right], \tag{6.2}$$

where $t = 4\alpha\gamma/\beta^2 = 4\gamma(T - T_0)/\varepsilon_0 C\beta^2$ is the reduced temperature, $P_0 = \sqrt{-\beta/\gamma}$ is the spontaneous polarization and $\chi_0 = \chi(T = T_0) = \gamma/2\beta^2$ is the ferroelectric contribution to the dielectric susceptibility, both evaluated at $t = 0$ ($T = T_0$). The linear approximation in Eqn (6.1) is adequate over the entire temperature range shown by the solid line in Fig. 20. The intrinsic coercive field is about one tenth of the depolarization field $P_0/\chi_0$, the internal electric field in the absence of surface charges. The data in Fig. 20 were obtained from measurements of the butterfly curves on a 30-ML film in a wide range of temperatures. The solid line is a plot of the theoretical prediction for $E_c(T)$ (6.1), (6.2) fitting only the slope $P_0/\chi_0$ to the data; the values of $T_0$ (34 °C), $C$ and $\beta$ used to calculate the reduced temperature $t$ were obtained from independent measurements of the dielectric constant [68], transition temperature [68], and critical point [72]. Table 3 gives these data both for LB and spun films. The excellent agreement of the calculated (solid line) and measured values (squares) of $E_c$ in Fig. 20 confirms that it is the intrinsic coercive field that is being measured.

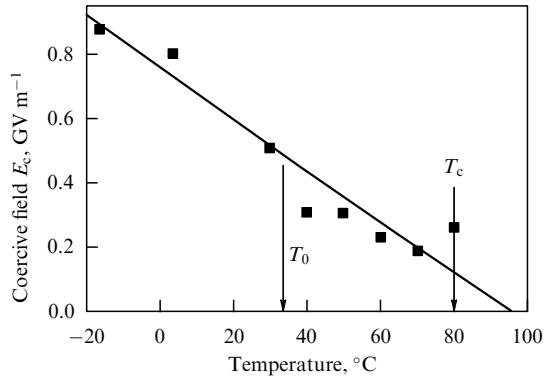


**Figure 20.** Temperature dependence of the intrinsic coercive field $E_c$ (solid line) and experimental values of $E_c$, measured for a 30-ML P(VDF–TrFE 70 : 30) LB film [90].

What is the reason for the transition from the nucleation-limited extrinsic coercive field to the nucleation-independent extrinsic coercive field at 15-nm thickness? Even the thinnest spun ferroelectric films of 60 nm reached a coercive field of only $E_c \approx 0.1$ GV m$^{-1}$ [7], still well below the intrinsic coercive field of 0.5 GV m$^{-1}$ calculated from Eqn (3). More recent studies of the dependence of the size effect in LB

**Table 3.** Landau–Ginzburg coefficients for P(VDF–TrFE) copolymers.

| Constants | LB Films, copolymer 70 : 30 | Bulk film, copolymer 65 : 35 [40] |
|---|---|---|
| Curie constant $C$ | $1500 \pm 300$ K [68] | 3227 K |
| Curie temperature $T_0$ | $+30 \pm 7\,^{\circ}$C [72] | $+40\,^{\circ}$C |
| Phase transition temperature $T_c$ | $+78 \pm 2\,^{\circ}$C [68, 72] | $+102\,^{\circ}$C |
| Spontaneous polarization $P_s$ | 0.1 C m$^{-2}$ | 0.1 C m$^{-2}$ |
| $\beta$, m$^5$ C$^{-2}$ F$^{-1}$ | $(-1.1 \pm 0.3) \times 10^{12}$ | $-1.5 \times 10^{12}$ |
| $\gamma$, m$^9$ C$^{-4}$ F$^{-1}$ | $(6.2 \pm 1.5) \times 10^{13}$ | $1.9 \times 10^{14}$ |

ferroelectric copolymer films on thickness confirm the size effect in the thickness range of 18 to 60 nm [74]. This behavior is consistent with the dominance of the nucleation mechanism; as the films become thinner, the nucleation volume is reduced and becomes energetically less favorable [91, 92] until it is completely inhibited.

The present results lead to the following conclusions. First, there is no apparent critical thickness in LB ferroelectric films as thin as 1 nm, much thinner than any previous ferroelectric films. Second, there is no finite-size effect in LB ferroelectric films with a thickness in the interval 1 – 15 nm, contrary to the predictions detailed in Section 2. Therefore, these LB ferroelectric films must be considered essentially two-dimensional ferroelectrics. Third, in the region of two-dimensionality these films reveal the intrinsic coercive field, which means that ferroelectric switching essentially does not include the usual nucleation and domain propagation processes. The real mechanism of this intrinsic switching is still not known.

The two-dimensional nature of the LB films means that the ferroelectric state may be generated by coupling only within the plane of the film. Any coupling between planes is weak and possibly responsible for the lower surface layer transition temperature. The Ising model for ultrathin films [36] is a more appealing approach to modeling ferroelectricity in two-dimensional polymer films because the dipole moments have restricted freedom — they can rotate only about the chain axis and are further inhibited from rotations about the axis by both interchain steric interactions and intrachain dihedral stiffness. We expect that an appropriate Ising model could be constructed in two ways. First, with the use of anisotropic coupling constants (like the exchange integrals in ferromagnetism) with strong ferroelectric coupling in the plane and a weak coupling perpendicular to the plane. Second, with the use of a purely two-dimensional model and making a weak interplanar coupling through a mean-field shared by all layers. Both approaches can achieve ferroelectricity at finite temperature in a single layer and either enhancement or suppression by neighboring layers or electrodes, depending on the sign of the interlayer coupling. Both approaches also suggest that the surface layers, boundaries between the ferroelectric film, and the electrodes or other outside material have a Curie point different from the interior 'bulk' layers because they couple with only one other ferroelectric layer. Fluctuations in two dimensions are not expected to destroy ordering as in the case of the isotropic Heisenberg ferromagnet [3] because the coupling is intrinsically anisotropic, and the polymer dipoles have only one rotational degree of freedom, compared to the two rotational degrees of freedom of the magnetic dipoles.

## 7. The surface phase transition in ferroelectric films

It was proposed in Ref. [68] that the phase transition in ferroelectric LB films at $\sim 20\,^{\circ}\mathrm{C}$ has a surface character. Surface phase transitions are known and were observed in ferromagnetic materials [4] and in silicon at the surface nonmetal-to-metal transition [93, 94] †.

† In the recent papers the surface phase transitions were observed in the crystals of Si and Ge, see Li D et al. *Phys. Rev. Lett.* **72** 3112 (1994), Gavioli L, Betti M G, Mariani C *Phys. Rev. Lett.* **77** 3869 (1996) (*Authors' note for English Edition.*)

The surface nature of the low-temperature first-order phase transition in P(VDF – TrFE) LB films was verified by means of several surface-sensitive spectroscopies, such as photoemission spectroscopy, angle-resolved inverse photoemission spectroscopy, and work function measurements. Here we summarize these data [69, 71, 95, 96].

The angle-resolved inverse photoemission spectroscopy clearly shows the change in the surface band structure at $+20\,^{\circ}\mathrm{C}$. First, there is a drastic change in the unoccupied density of states at the Fermi level. Second, there is a doubling of the surface Brillouin zone at this temperature, as shown in Fig. 10d. Figure 10d [69] schematically shows the Brillouin zone of the surface phase at $T < 20\,^{\circ}\mathrm{C}$ (thick lines), with the zone center denoted by a circle. The Brillouin zone for $T > 20\,^{\circ}\mathrm{C}$ is correspondingly represented by thin lines and the various Brillouin zone centers are denoted by squares. These data were obtained for 5-ML P(VDF – TrFE 70 : 30) LB films deposited directly on Si substrates. The data show that the phase transition from the upper phase to the lower one is accompanied by the doubling of the Brillouin zone. Along the $a_1$ high symmetry direction of the surface Brillouin zone (the direction parallel to the polymer chains), the distance between zone centers decreases from $1.30 \pm 0.04$ A to $0.73 \pm 0.05$ A. There occurs an increase in the density of states at the Fermi level and a shift of the unoccupied states of the conduction band toward the Fermi level. The increase in the work function, which suggests a structural change leading to a reorientation of the surface H – F dipoles toward the surface, is consistent with these observations.

The results obtained in Refs [69, 71, 95, 96] lead to the conclusion that the surface phase transition in LB films of P(VDF – TrFE) is associated with a rotation of the polar groups about the molecular chain axis and is connected with the transition of the all-trans structure into the trans – gauche structure. It is the same structure change that was identified for the bulk phase transition in spun films [42]. Thus, at $20\,^{\circ}\mathrm{C}$ the surface of the films undergoes a phase transition of the first order, perhaps antiferroelectric ordering, but there is no apparent change in the observed electronic band symmetries.

## 8. Conclusions

LB technology permits us to obtain ultrathin ferroelectric films that show two-dimensional behavior. For LB ferroelectric films prepared from the P(VDF – TrFE) copolymer, there is no critical thickness, contrary to the predictions of the three-dimensional mean-field theory. This does not mean that the critical size or thickness does not exist in other ferroelectric crystals or films.

The ferroelectric surface phase transition was observed for the first time in copolymer LB films. How many monolayers are involved in the surface phase transition is still unknown. Maybe the method of X-ray standing waves will help to answer this question. These results do not exclude the existence of surface phase transitions in other ferroelectrics.

**Acknowledgments**

We thank V L Ginzburg for his interest and the proposal to write this review. The authors are also grateful to E G Maksimov for useful comments. The work at the University of Nebraska was supported by the U.S. National Science Foundation, the U.S. Office of Naval Research, the

U.S. Air Force Office of Scientific Research, and the Nebraska Research Initiative through the Center for Materials Research and Analysis. Work at the Institute of Crystallography was supported by INTAS.

## References


1. Dürr W et al. *Phys. Rev. Lett.* **62** 206 (1989)
2. Farle M, Baberschke K *Phys. Rev. Lett.* **58** 511 (1987)
3. Mermin N D, Wagner H *Phys. Rev. Lett.* **17** 1133 (1966)
4. Dowben P A, McIlroy D N, Li D, in *Handbook on the Physics and Chemistry of Rare Earths* Vol. 24 (Eds J K A Gschneidner, L Eyring) (Amsterdam: Elsevier, 1997) Ch. 159
5. Ishikawa K, Yoshikawa K, Okada N *Phys. Rev. B* **37** 5852 (1988)
6. Tanaka M, Makino Y *Ferroelectrics Lett.* **24** 13 (1998)
7. Kimura K, Ohigashi H *Jpn. J. Appl. Phys.* **25** 383 (1986)
8. Scott J F *Phase Transitions* **30** 107 (1991)
9. Tilley D R, in *Ferroelectric Thin Films*: *Synthesis and Basic Properties* (Eds C Paz de Araujo, J F Scott, G F Taylor) (Amsterdam: Gordon and Breach, 1996) p. 11
10. Scott J F *Physica B* **150** 160 (1988)
11. Onsager L *Phys. Rev.* **65** 117 (1944)
12. Valasek J *Phys. Rev.* **15** 537 (1920)
13. Devonshire A F *Adv. Phys.* **3** 85 (1954)
14. Lines M E, Glass A M *Principles and Applications of Ferroelectrics and Related Materials* (Oxford: Clarendon, 1977)
15. Fridkin V M *Ferroelectric Semiconductors* (New York: Consultants Bureau, 1980)
16. Valasek J *Phys. Rev.* **17** 475 (1921)
17. Blinc R, Zeks B *Soft Modes in Ferroelectrics and Antiferroelectrics* (Amsterdam: North-Holland, 1974)
18. Xu Y *Ferroelectric Materials and Their Applications* (Amsterdam: North-Holland, 1991)
19. Strukov B A, Levanyuk A P *Ferroelectric Phenomena in Crystals* (Berlin: Springer-Verlag, 1998)
20. Ginzburg V L *Zh. Eksp. Teor. Fiz.* **15** 739 (1945) [*J. Phys. USSR* **10** 107 (1946)]
21. Ginzburg V L *Zh. Eksp. Teor. Fiz.* **19** 36 (1949)
22. Landau L D, Lifshitz E M *Statistical Physics* Part I (Oxford: Pergamon, 1980)
23. Landau L D *Zh. Eksp. Teor. Fiz.* **7** 627 (1937); *Phys. Z. Sowjetunion* **11** 545 (1937)
24. Landau L D *Phys. Z. Sowjetunion* **11** 545 (1937)
25. Devonshire A F *Philos. Mag.* **40** 1040 (1949)
26. Devonshire A F *Philos. Mag.* **42** 1065 (1951)
27. Gerzanich E I, Fridkin V M *Pis'ma Zh. Eksp. Teor. Fiz.* **8** 553 (1968) [*JETP Lett.* **8** 337 (1968)]
28. Strukov B A, Amin M, Kopchik V A *Phys. Status Solidi* **27** 741 (1968)
29. Keve E T et al. *Commun. Solid State Phys.* **8** 1517 (1970)
30. Bahr C, Heppke G *Phys. Rev. A* **39** 5459 (1989)
31. Cottam M G, Tilley D R, Zeks B *J. Phys. C* **17** 1793 (1984)
32. Tilley D R *Phase Transitions in Thin Films in Ferroelectric Ceramics* (Basel: Birkhäuser, 1993)
33. Duiker H M "Static and dynamic properties of ferroelectric thin film memories" PhD Thesis (University of Colorado, 1989)
34. Qu B D et al. *Ferroelectrics* **152** 219 (1994)
35. Scott J F et al. *Phys. Rev. B* **35** 4144 (1987)
36. Wang C L, Zhong W L, Zhang P L *J. Phys.*: *Condens. Matter* **3** 4743 (1992)
37. Li S et al. *Phys. Lett. A* **212** 341 (1996)
38. Li S et al. *Philos. Mag. B* **76** 47 (1997)
39. DeGennes P G *Solid State Commun.* **1** 132 (1963)
40. Furukawa T *Ferroelectrics* **57** 63 (1984)
41. Furukawa T *Phase Transitions* **18** 143 (1989)
42. Lovinger A J *Science* **220** 1115 (1983)
43. Lovinger A J, in *Developments in Crystalline Polymers* Vol. 1 (Ed. D C Basset) (London: Elsevier Applied Science, 1982)
44. Wang T T, Herbert J M, Glass A M *The Applications of Ferroelectric Polymers* (New York: Chapman and Hall, 1988)
45. Nalwa H S *Ferroelectric Polymers* (New York: Marcel Dekker, 1995)
46. Sessler G M (Ed.) *Electrets* (Berlin: Springer-Verlag, 1980)
47. Furukawa T, Date M, Fukada E *Ferroelectrics* **57** 63 (1980)
48. Yagi T, Tatemoto M, Sako J *Polymer J.* **12** 209 (1980)
49. Lovinger A J *Macromolecules* **16** 1529 (1983)
50. Verkhovskaya K A, Danz R, Fridkin V M *Fiz. Tverd. Tela* **29** 2198 (1987) [*Sov. J. Solid State* **29** 1268 (1987)]
51. Berry M H, Gookin D N, in *Nonlinear Optical Properties of Organic Materials* (Proc. SPIE, Vol. 971, Ed. G Khanarian) (Bellingham, Wash.: SPIE, 1988) p. 154
52. Bergman J G, McFee J H, Crane G R *Appl. Phys. Lett.* **18** 203 (1971)
53. Verkhovskaya K A et al. *Ferroelectrics* **134** 7 (1992)
54. Litt M H, Hsu C, Basu P *J. Appl. Phys.* **48** 2208 (1977)
55. Esayan S, Scheinbeim J I, Newman B A *Appl. Phys. Lett.* **67** 623 (1995)
56. Hachiya S *J. Soc. Inform. Disp.* **1** 295 (1993)
57. Fernandez M V, Suzuki A, Chiba A *Macromolecules* **20** 1806 (1987)
58. Tashiro K, Takano K, Kobayashi M *Ferroelectrics* **57** 297 (1984)
59. Palto S et al. *Ferroelectrics Lett.* **19** 65 (1995)
60. Bune A et al. *Appl. Phys. Lett.* **67** 3975 (1995)
61. Blinov L M *Usp. Fiz. Nauk* **155** 443 (1988) [*Sov. Phys. Usp.* **31** 623 (1988)]
62. Roberts G G *Langmuir–Blodgett Films* (New York: Plenum, 1990)
63. Petty M C *Langmuir–Blodgett Films*: *An Introduction* (Cambridge: Cambridge University Press, 1996)
64. Ducharme S et al. *Ferroelectrics* **202** 29 (1997)
65. Advincula R C et al., in *Organic Thin Films*: *Structure and Applications* (ACS Symposium Series, Vol. 695, Ed. C W Frank) (Washington, DC: American Chemical Society, 1998) p. 192
66. Sorokin A V "Langmuir–Blodgett deposition of ferroelectric polymer films" PhD Thesis (Moscow: Institute of Crystallography, 1997)
67. Palto S et al. *Europhys. Lett.* **34** 465 (1996)
68. Bune A et al. *Nature* (London) **391** 874 (1998)
69. Choi J et al. *Phys. Lett. A* **249** 505 (1999)
70. Borca C N et al. *Appl. Phys. Lett.* **74** 347 (1999)
71. Choi J et al. *Phys. Rev. B* **61** 5760 (2000)
72. Ducharme S et al. *Phys. Rev. B* **57** 25 (1998)
73. Legrand J F *Ferroelectrics* **91** 303 (1989)
74. Blinov L M et al. *Thin Solid Films* **284–285** 474 (1996)
75. Sorokin A V et al. *Mol. Mater.* **6** 61 (1996)
76. Bune A V et al. *J. Appl. Phys.* **85** 7869 (1999)
77. Merz W J *Phys. Rev.* **91** 513 (1953)
78. Okada K, Sugie H *Phys. Lett. A* **37** 337 (1971)
79. Gladkiĭ V V, Sidnenko E V *Fiz. Tverd. Tela* **13** 3092 (1971) [*Sov. J. Solid State* **13** 2592 (1971)]
80. Kawai H *Jpn. J. Appl. Phys.* **8** 975 (1969)
81. Tashiro K et al. *Macromol.* **13** 691 (1980)
82. Fukada E *Phase Transitions* **18** 135 (1989)
83. Furukawa T, Seo N *Jpn. J. Appl. Phys.* **24** 675 (1990)
84. Nye P *Physical Properties of Crystals* (London: Oxford Press, 1967)
85. Fowler R H, Nordheim L *Proc. R. Soc. London. Ser. A* **119** 173 (1928)
86. Isono Y, Nakano H *J. Appl. Phys.* **75** 4557 (1994)
87. Wang C L et al. *Phys. Lett. A* **254** 297 (1999)
88. Furukawa T et al. *Jpn. J. Appl. Phys.* **24** L661 (1985)
89. Allenspach R, Bishof A *Phys. Rev. Lett.* **69** 3385 (1992)
90. Ducharme S et al. *Phys. Rev. Lett.* **84** 175 (2000)
91. Tagantsev A K *Integr. Ferroelectrics* **16** 237 (1997)
92. Tagantsev A K *Ferroelectrics* **184** 79 (1996)
93. Kevan S D, Stoffel N G *Phys. Rev. Lett.* **53** 702 (1984)
94. Kevan S D *Phys. Rev. B* **32** 2344 (1985)
95. Choi J et al. *Phys. Rev. Lett.* **80** 1328 (1998)
96. Choi J et al. *Phys. Rev. B* **59** 1819 (1998)
97. Kohler R et al. *J. Korean Phys. Soc.* **32** 1744 (1998)